



## Combining Face Averageness and Symmetry for 3D-based Gender Classification

Baiqiang Xia, Boulbaba Ben Amor, Hassen Drira, Mohamed Daoudi,  
Lahoucine Ballihi

### ► To cite this version:

Baiqiang Xia, Boulbaba Ben Amor, Hassen Drira, Mohamed Daoudi, Lahoucine Ballihi. Combining Face Averageness and Symmetry for 3D-based Gender Classification. Pattern Recognition, 2015, 48 (3), pp.746-758. hal-01074090

**HAL Id: hal-01074090**

**<https://hal.science/hal-01074090>**

Submitted on 12 Oct 2014

**HAL** is a multi-disciplinary open access archive for the deposit and dissemination of scientific research documents, whether they are published or not. The documents may come from teaching and research institutions in France or abroad, or from public or private research centers.

L'archive ouverte pluridisciplinaire **HAL**, est destinée au dépôt et à la diffusion de documents scientifiques de niveau recherche, publiés ou non, émanant des établissements d'enseignement et de recherche français ou étrangers, des laboratoires publics ou privés.

# Combining Face Averageness and Symmetry for 3D-based Gender Classification

Baiqiang Xia, Boulbaba Ben Amor, Hassen Drira, Mohamed Daoudi, and  
Lahoucine Ballihi.

---

## Abstract

Although human face averageness and symmetry are valuable clues in social perception (such as attractiveness, masculinity/femininity, healthy/sick, etc.), in the literature of facial attribute recognition, little consideration has been given to them. In this work, we propose to study the morphological differences between male and female faces by analyzing the averageness and symmetry of their 3D shapes. In particular, we address the following questions: (i) is there any relationship between gender and face averageness/symmetry? and (ii) if this relationship exists, which specific areas on the face are involved? To this end, we propose first to capture densely both the face shape averageness (AVE) and symmetry (SYM) using our Dense Scalar Field (DSF), which denotes the shooting directions of geodesics between facial shapes. Then, we explore such representations by using classical machine learning techniques, the Feature Selection (FS) methods and Random Forest (RF) classification algorithm. Experiments conducted on the FRGCv2 dataset show a significant relationship exists between gender and facial averageness/symmetry when achieving a classification rate of 93.7% on the 466 earliest scans of subjects (mainly neutral) and 92.4% on the whole

FRGCv2 dataset (including facial expressions).

*Keywords:*

3D Face, Gender Classification, Face averageness, Face symmetry, Dense Scalar Field, Feature selection, Random Forest.

---

## 1. Introduction

Human gender perception is an extremely reliable and fast cognitive process since the face presents a clear sexual dimorphism [1]. In human face analysis using machines [3], automatic gender classification is an active research area. Developed solutions could be useful in human computer interaction (intelligent user interface, video games, etc.), visual surveillance, collecting demographic statistics for marketing (audience or consumer proportion analysis, etc.), and security industry (access control, etc.). Research on automatic gender classification using facial images goes back to the beginning of the 1990s. Since then, significant progress has been reported in the literature [4, 5, 6, 7, 8]. Fundamentally, proposed techniques differ in (i) the format of facial data (2D still images, 2D videos or 3D scans); (ii) the choice of facial representation, ranging from simple raw 2D pixels or 3D cloud of points to more complex features, such as Haar-like, LBP and AAM in 2D, and shape index, wavelets and facial curves in 3D; and (iii) the classifiers, for instance Neural Networks, SVM, and Boosting methods [4].

### 1.1. Related work on 3D-based gender classification

Statistically, the male and the female faces present different morphological characteristics in geometrical features, such as in the hairline, the forehead, the eyebrows, the eyes, the cheeks, the nose, the mouth, the chin, the jaw, the

21 neck, the skin and the beard regions [13]. Usually, the female brow tends to be  
22 more arched than that of the male (which is more horizontal), the noses and  
23 chins in male faces are more prominent than those in female faces [27], and  
24 men have a more acute nasolabial angle than women [26]. The 3D face scans,  
25 which capture the spatial structure of the facial surfaces, allow to capture  
26 these differences between male and female faces more easily compared to 2D  
27 texture images. Thus, the goal of 3D-based gender classification is to develop  
28 a fast and automatic approach which yields high classification performance  
29 compared to the 2D-based approaches.

30 In [9], *Liu et al.* analyze the relationship between facial asymmetry and  
31 gender. They impose a 2D grid on each 3D face to represent the face with  
32 3D grid points. With the selected symmetry plane, which equally separates  
33 the face into right and left halves, the distance difference between each point  
34 and its corresponding reflected point is calculated as height differences (HD).  
35 In addition, the angle difference between their normal vectors is calculated  
36 as orientation differences (OD). The approach based on HD-face achieves  
37 91.16% and the approach based on OD-face achieves 96.22%. However, these  
38 performances are reported on a private dataset of 111 full 3D neutral face  
39 models of 111 subjects, and 3D face manual landmarks are needed.

40 In [12], *Lu et al.* use Support Vector Machine (SVM) to classify ethnicity  
41 (Asian and Non-Asian) and gender (Male and Female). A merging of two  
42 frontal 3D face databases (UND and MSU databases) is used for the exper-  
43 iments. The best gender classification results using 10-fold cross-validation  
44 reported is 91%. However, this approach is based on six landmarks (inside  
45 and outside corners of the eyes, the nose tip, and the chin point) manually

46 labeled. Moreover, the results are obtained only on neutral faces.

47 In [15], *Wu et al.* use 2.5D facial surface normals recovered with Shape  
48 From Shading (SFS) from intensity images for gender classification. The  
49 best average gender recognition rate reported is 93.6% with both shape and  
50 texture considered. However, seven manual landmarks are needed and a  
51 small dataset of neutral scans has been used to perform the experiments.

52 In [16], *Hu et al.* propose a fusion-based gender classification method  
53 from 3D frontal faces. Each 3D face shape is separated into four face regions  
54 using face landmarks. With the extracted features from each region, the  
55 classification is done using SVM on a subset of the UND dataset and another  
56 database captured by themselves. Results show that the upper region of  
57 the face contains the highest amount of discriminating gender information.  
58 Fusion is applied to the results of four face regions and the best result reported  
59 is 94.3%. Their experiments only involve neutral faces. In this study, no  
60 attention is given to facial expressions.

61 In [3], *Toderici et al.* employ MDS (Multi-Dimensional Scaling) and  
62 wavelets on 3D face meshes for gender classification. They use the 4007  
63 3D scans of the 466 subjects from the FRGCv2 dataset for gender classifi-  
64 cation. Experiments are carried out subject-independently with no common  
65 subject used in the testing stage of 10-fold cross validation. With polynomial  
66 kernel SVM, they achieve 93% gender classification rate with the unsuper-  
67 vised MDS approach, and 94% classification rate with the wavelets-based  
68 approach. Both approaches significantly outperform the kNN and kernel-  
69 kNN approaches.

70 In [17], *Ballihi et al.* extract facial curves (26 level curves and 40 radial

71 curves) from 3D faces for gender classification. The features are extracted  
 72 from lengths of geodesics between facial curves from a given face to the Male  
 73 and Female templates computed using the Karcher Mean Algorithm. The  
 74 Adaboost algorithm is then used to select salient facial curves. They obtained  
 75 a classification rate of 84.12% with the nearest neighbor classifier when using  
 76 the 466 earliest scans of the FRGCv2 dataset as the testing set. They also  
 77 performed a standard 10-fold cross-validation for the 466 earliest scans of  
 78 FRGCv2, and obtain 86.05% with Adaboost.

79 Compared to [17], in the current paper, we represent mathematically fa-  
 80 cial bilateral symmetry and averageness for gender classification using Dense  
 81 Scalar Fields. The DSFs denoting the shooting directions for geodesics be-  
 82 tween facial shapes, are both novel and interesting. We view this representa-  
 83 tion for gender classification as the main contribution of this paper. The set  
 84 of facial deformations is a nonlinear space while the set of Dense Scalar Field  
 85 (DSF) is a vector space. The only remaining challenge is the large dimen-  
 86 sionality of DSF, which is handled using a feature-selection-based dimension  
 87 reduction, followed by a Random Forest classifier. In terms of experimental  
 88 performances, the present approach have achieved higher classification rates  
 89 compared to [17]. In summary, the novelty of this paper is in represent-  
 90 ing bilateral symmetry and face averageness using DSF and its successful  
 91 application to the gender classification problem.

## 92 1.2. Methodology and contributions

93 From the above analysis, existing works on 3D-based gender classification  
 94 are based on local or global *low-level* feature extraction (see table 2 for a  
 95 complete summary) followed by classical classification methods. To the best

of our knowledge, no work has been done considering *high-level* cues, such as face averageness and bilateral face symmetry, except the study in [9] which investigates the relationship between facial symmetry and gender. Using sparse measures of height differences (HD), and orientation differences (OD) on a defined grid imposed on full 3D face models, their process requires manual landmarks on the face and the experiments are performed on a small dataset. The main contributions of this work are as follows :

☞ We introduce two *high-level* features, face averageness (AVE) and bilateral face symmetry (SYM), for 3D-based gender classification. These primary facial perception features are rarely considered in the literature of facial attribute recognition.

☞ We provide an interesting mathematical tool, named *Dense Scalar Field* (DSF) [18], to capture densely and quantitatively the averageness/symmetry differences on the face surface. The DSFs grounding on Riemannian shape analysis are capable to densely capture the shape differences in 3D faces (such as averageness/symmetry differences).

☞ We propose a fully-automatic gender classification without any human interaction. We achieve competitive results compared to the approaches in the state-of-the-art on a challenging dataset, FRGCv2. Also, we provide a comprehensive study of the robustness of the proposed approach against age, ethnicity and expression variations.

An overview of the proposed approach is shown in Figure 1. Firstly, during the first step an algorithm commonly used for facial scans preprocessing is applied. It includes hole filling, facial part cropping and 3D mesh smoothing

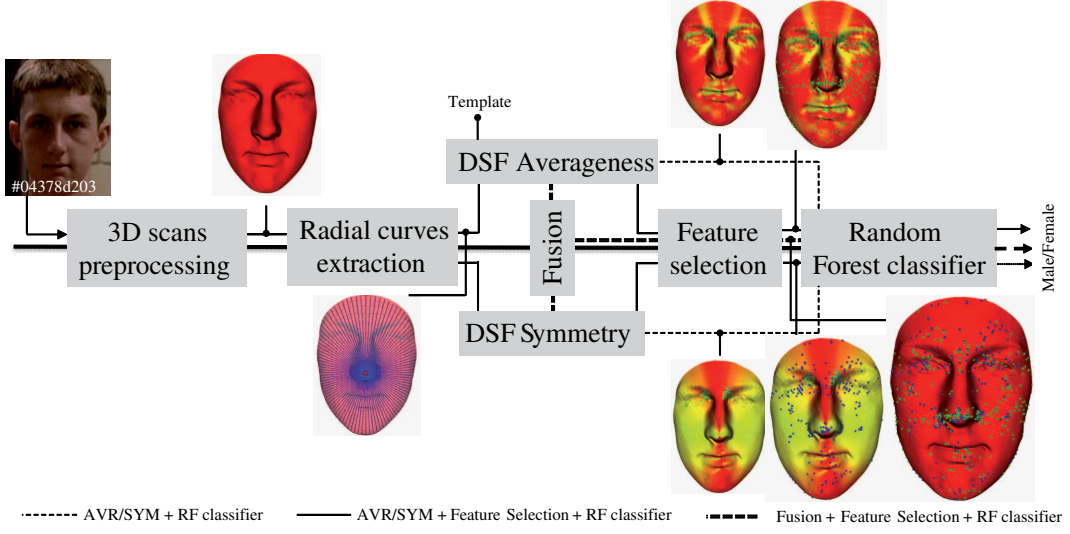


Figure 1: Flow chart of the proposed gender classification approach. There are various pipelines for gender classification. Namely, the pipelines are, (1) the symmetry DSF features (*SYM-Original*), (2) the selected features of symmetry DSF features (*SYM-Selection*), (3) the averageness DSF features (*AVE-Original*), (4) the selected features of averageness DSF features (*AVE-Selection*), (5) the fusion of symmetry and averageness DSF features by concatenation (*FUS-Original*), and (6) the selected features of the fusion of symmetry and averageness DSF features (*FUS-Selection*).

120 applied to each scan, together with nose tip detection and pose normaliza-  
 121 tion, as proposed in [17] or [12]. We denote the preprocessed face as  $\mathbf{S}$ . The  
 122 plane which equally separates the preprocessed face  $\mathbf{S}$  into right and left  
 123 halves is picked up as the middle plane. This plane  $P(t, \vec{n}_h)$  passes through  
 124 the detected nose tip  $t$  and has a horizontal normal  $\vec{n}_h$  from the frontal view.  
 125 Secondly, a DSF extraction step goes after the preprocessing. Here, the pre-  
 126 processed face  $\mathbf{S}$  is approximated by a collection of radial curves defined over  
 127 the facial region and stemming from the nose tip. Then, the *Dense Scalar*  
 128 *Field* (DSF) features are computed, pair-wisely, to capture the shape dif-



129 ferences (averageness/symmetry differences) between corresponding radial  
 130 curves on each indexed point. Thus, we obtain two DSFs for each scan, an  
 131 averageness DSF and a symmetry DSF. A fusion descriptor is then obtained  
 132 for each scan by concatenating its averageness DSF and symmetry DSF.  
 133 Thirdly, after DSF extraction, we investigate the two following classification  
 134 pipelines. In the first pipeline, Random Forest classifier is applied directly  
 135 on the obtained feature vectors - averageness DSFs, symmetry DSFs and  
 136 fusion DSFs. In the second pipeline, we first apply a supervised feature se-  
 137 lection (FS) algorithm on the averageness, symmetry and their fusion DSFs,  
 138 then the Random Forest (RF) classifier is applied on the selected features for  
 139 gender classification.

140 This work relates closely to the work previously published in [17], in terms  
 141 of face representation by an indexed collection of radial curves, which is one  
 142 of the first steps of our approach’s pipeline. However, while this face param-  
 143 eterization is in common, the feature extraction step is completely different.  
 144 Indeed, in [17], the features are extracted from *lengths of geodesics* be-  
 145 tween facial curves from a given face to the Male and Female templates. In  
 146 contrast, this work considers the *shooting vectors on the geodesics* be-  
 147 tween facial curves to capture shape differences. The DSFs are computed to  
 148 describe densely the *Symmetry* and *Averageness* of a given face. This allows  
 149 to compute densely and locally the facial features on each point of the  
 150 face.

151 The rest of the paper is organized as follows: in section **2**, we high-  
 152 light our methodology for extracting features that contain 3D facial avera-  
 153 geness/symmetry difference; in section **3**, we detail the classifier, the feature

selection method, and the fusion method for gender classification; experimental results and discussions are presented in section 4 while section 5 concludes the work.

## 2. Feature Extraction Methodology

As mentioned earlier, after the preprocessing, the next step of our approach is to extract densely the averageness and symmetry features from faces. Both of them are based on a Riemannian shape analysis of 3D face.

### 2.1. Background on Dense Scalar Field Computation

The idea to capture locally and densely face asymmetry and its averageness is to represent facial surface  $\mathbf{S}$  by a set of parameterized radial curves emanating from the nose tip  $\mathbf{t}$ . Such an approximation can be seen as a solution to facial surface parameterization which approximates the local shape information. Then, a Dense Scalar Field (DSF), based on pairwise shape comparison of corresponding curves, is computed along these radial curves on each point. A similar framework has been used in [18] for 4D face expression recognition by quantifying deformations across 3D face sequences followed by a classification technique. More formally, a parametrized curve on the face,  $\beta : I \rightarrow \mathbb{R}^3$ , where  $I = [0, 1]$ , is represented mathematically using the *square-root velocity function* [19], denoted by  $q(t)$ , according to:  $q(t) = \frac{\dot{\beta}(t)}{\sqrt{\|\dot{\beta}(t)\|}}$ . This specific parameterization has the advantage of capturing the shape of the curve and providing simple calculus [19].

Let us define the space of such functions:  $\mathcal{C} = \{q : I \rightarrow \mathbb{R}^3, \|q\| = 1\} \subset \mathbb{L}^2(I, \mathbb{R}^3)$ , where  $\|\cdot\|$  implies the  $\mathbb{L}^2$  norm. With the  $\mathbb{L}^2$  metric on its tangent spaces,  $\mathcal{C}$  becomes a Riemannian manifold. Given two curves  $q_1$  and  $q_2$ , let  $\psi$

178 denote a path on the manifold  $\mathcal{C}$  between  $q_1$  and  $q_2$ ,  $\dot{\psi} \in T_{\psi}(\mathcal{C})$  is a tangent  
 179 vector field along the path  $\psi \in \mathcal{C}$ . In our case, as the elements of  $\mathcal{C}$  have a  
 180 unit  $\mathbb{L}^2$  norm,  $\mathcal{C}$  is a hypersphere of the Hilbert space  $\mathbb{L}^2(I, \mathbb{R}^3)$ . The geodesic  
 181 path  $\psi^*$  between any two points  $q_1, q_2 \in \mathcal{C}$  is simply given by the minor arc  
 182 of great circle connecting them on this hypersphere,  $\psi^* : [0, 1] \rightarrow \mathcal{C}$ , given  
 183 by:

$$\psi^*(\tau) = \frac{1}{\sin(\theta)} (\sin((1 - \tau)\theta)q_1 + \sin(\theta\tau)q_2) \quad (1)$$

184 and  $\theta = d_{\mathcal{C}}(q_1, q_2) = \cos^{-1}(\langle q_1, q_2 \rangle)$ . We point out that  $\sin(\theta) = 0$  if the  
 185 distance between the two curves is null, in other words  $q_1 = q_2$ . In this case,  
 186 for each  $\tau$ ,  $\psi^*(\tau) = q_1 = q_2$ . The tangent vector field along this geodesic  
 187  $\dot{\psi}^* : [0, 1] \rightarrow T_{\psi}(\mathcal{C})$  is given by (2):

$$\dot{\psi}^* = \frac{d\psi^*}{d\tau} = \frac{-\theta}{\sin(\theta)} (\cos((1 - \tau)\theta)q_1 - \cos(\theta\tau)q_2) \quad (2)$$

188 Knowing that on a geodesic, the covariant derivative of its tangent vector  
 189 field is equal to 0,  $\dot{\psi}^*$  is parallel along the geodesic  $\psi^*$  and we shall represent it  
 190 with  $\dot{\psi}^*|_{\tau=0}$ . This vector  $\dot{\psi}^*|_{\tau=0}$  represents the initial velocity of the geodesic  
 191 path connecting  $q_1$  to  $q_2$  and called also the shooting vector for this geodesic.  
 192 Accordingly, (2) becomes:

$$\dot{\psi}^*|_{\tau=0} = \frac{\theta}{\sin(\theta)} (q_2 - \cos(\theta)q_1) \quad (3)$$

193 with  $\theta \neq 0$ . Thus,  $\dot{\psi}^*|_{\tau=0}$  is sufficient to represent this vector field; the  
 194 remaining vectors can be obtained by parallel transport of  $\dot{\psi}^*|_{\tau=0}$  along the  
 195 geodesic  $\psi^*$ . with the magnitude of  $\dot{\psi}_{\alpha}^*$  at each point, located in curve  $\beta_{\alpha}^S$

196 with index  $k$ , we build a *Dense Scalar Field* (DSF) on the facial surface  $\mathbf{S}$ ,  
 197  $V_\alpha^k = |\dot{\psi}_\alpha^*|_{(\tau=0)}(k)|$ . This *Dense Scalar Field* quantifies the shape difference  
 198 between corresponding curves on each indexed point.

## 199 2.2. Face symmetry description

200 The idea of the face symmetry description is to capture the bilateral  
 201 symmetry difference in the face by DSF. Symmetry difference is defined as  
 202 the deformation from a face point to its corresponding symmetrical point  
 203 on the other side of face. In practice, symmetry DSF is calculated on each  
 204 indexed point of the corresponding symmetrical curves in the preprocessed  
 205 face  $\mathbf{S}$ . Let  $\beta_\alpha$  denote the radial curve that makes an angle  $\alpha$  with the  
 206 middle plane  $P_{\mathbf{S}}(t, \vec{n}_h)$  from the frontal view of  $\mathbf{S}$ , and  $\beta_{2\pi-\alpha}$  denotes the  
 207 corresponding symmetrical curve that makes an angle  $(2\pi-\alpha)$  with  $P_{\mathbf{S}}(t, \vec{n}_h)$ .  
 208 The tangent vector field  $\dot{\psi}_\alpha^*$  that captures the deformation from  $\beta_\alpha$  to  $\beta_{2\pi-\alpha}$   
 209 is then calculated. With the magnitude of  $\dot{\psi}_\alpha^*$  at each point, located in the  
 210 curve  $\beta_\alpha$  with index  $k$ , we build a *symmetry Dense Scalar Field* (symmetry  
 211 DSF) on the facial surface.

212 This *Dense Scalar Field* quantifies the shape difference between corre-  
 213 sponding symmetrical curves on each point of the preprocessed face  $\mathbf{S}$ . Some  
 214 examples illustrating this symmetry descriptor are shown in Figure 2. For  
 215 each subject, face in column (a) shows the 2D intensity image; column (b)  
 216 illustrates the preprocessed 3D face surface  $\mathbf{S}$ ; column (c) illustrates the the  
 217 3D face  $\mathbf{S}$  with extracted curves; column (d) shows the symmetry degree as  
 218 a color-map of the DSF mapped on  $\mathbf{S}$ . The color bar is shown in the up-  
 219 right corner. The hot colors mean the minimum difference (i.e. maximum  
 220 symmetry) and cold colors signify the maximum difference (i.e. minimum

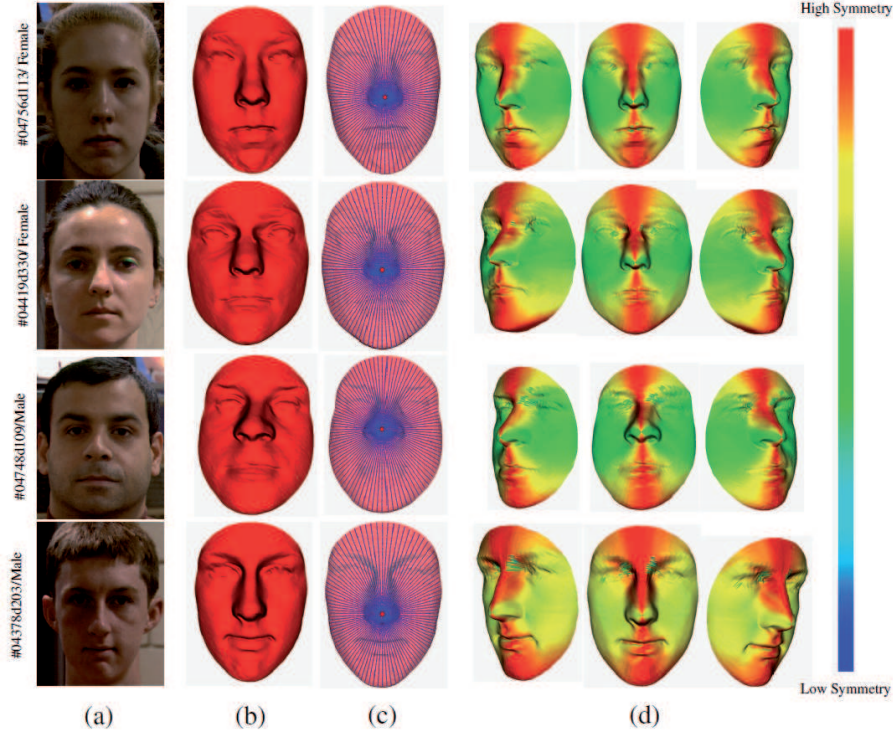


Figure 2: Illustrations of the symmetry DSFs on faces. (a) 2D intensity image; (b) preprocessed 3D face  $\mathcal{S}$ ; (c) 3D face  $\mathcal{S}$  with extracted curves; (d) color-map of symmetry DSF mapped on  $\mathcal{S}$  with three poses. While the cold colors reflect lower symmetrical regions, the warm colors represent higher symmetrical parts of the face.

221 symmetry). The hotter the color, the higher is magnitude of the bilateral  
 222 symmetry. In this work, the symmetry DSFs are generated with 200 radial  
 223 curves extracted from each face and 100 indexed points on each curve. Thus,  
 224 the size of each DSF is 20000. The average time consumed for extracting  
 225 all 200 curves for each face is 1.048 seconds, and for generating the bilateral  
 226 symmetry descriptor (symmetry DSF) on all the  $200 \times 100$  points of each  
 227 face is 0.058 seconds. The average preprocessing time consumed for each

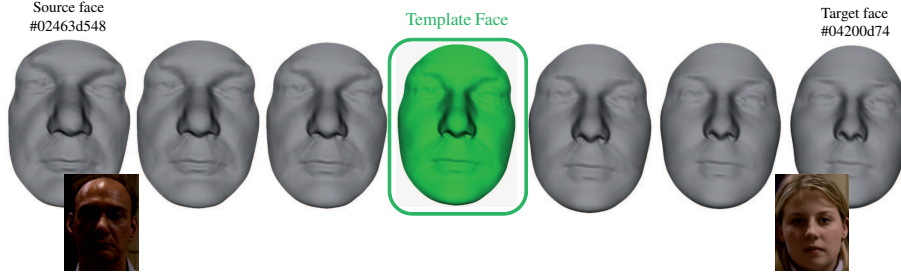


Figure 3: The averageness face template is defined as the middle point of the geodesic path between two representative faces randomly taken from the male and female classes in the FRGCv2 dataset.

scan is 0.116 seconds. The total computation time (including preprocessing)  
 for each scan is less than 1.25 seconds. All our programs are developed in  
 C++ and executed on Intel Core i5 CPU 2.53 GHZ with 4Go of RAM.

### 2.3. Face averageness description

As mentioned earlier, generally, male faces have more prominent features  
 (forehead, eyebrows, nose, mouth, etc.) in comparison with female faces.  
 Here, our aim is to capture the morphological sexual differences between  
 male and female faces by comparing their shape differences to a defined face  
 template. We assume that such differences change with the face gender.  
 Thanks to DSF, presented in subsection 2.1, we are able to capture densely  
 such shape differences as long as a face template is defined.

As shown in Figure 3, the face template is defined as the middle point  
 of the geodesic path which connects a male face (*ID: 02463d548; Age: 48; White*)  
 to a female face (*ID: 04200d74; Age: 21; White*) taken from the  
 FRGCv2 dataset. With the two faces represented by collections of radial  
 curves, we compute pair-wisely the geodesic path between corresponding

244 curves using equation (1). By interpolation, we have the middle point of the  
 245 geodesic which we take as the face template  $\mathbf{T}$ .

246 For a preprocessed face  $\mathbf{S}$ , let  $\beta_{\alpha}^{\mathbf{S}}$  denote the radial curve that makes  
 247 an angle  $\alpha$  with the middle plane  $P_{\mathbf{S}}(t, \vec{n}_h)$  from the frontal view of  $\mathbf{S}$ , and  
 248  $\beta_{\alpha}^{\mathbf{T}}$  denotes the curve that makes the same angle  $\alpha$  with  $P_{\mathbf{T}}(t, \vec{n}_h)$  in the  
 249 averageness face template  $\mathbf{T}$ . The tangent vector field  $\dot{\psi}_{\alpha}^*$  that represents the  
 250 projection of the deformation between the given face and the template face,  
 251 in the tangent space associated with the template face, is then calculated on  
 252 each point. Similar to the symmetry descriptor, with the magnitude of  $\dot{\psi}_{\alpha}^*$  at  
 253 each point, located in curve  $\beta_{\alpha}^{\mathbf{S}}$  with index  $k$ , we build an *averageness Dense*  
 254 *Scalar Field* (averageness DSF) on the facial surface,  $V_{\alpha}^k = |\dot{\psi}_{\alpha}^*|_{(\tau=0)}(k)|$ . This  
 255 *Dense Scalar Field* quantifies the shape difference between corresponding  
 256 curves of  $\mathbf{S}$  and  $\mathbf{T}$  on each indexed point.

257 Figure 4 shows this averageness descriptor. For each subject, the face in  
 258 column (a) shows the 2D intensity image; column (b) illustrates the prepro-  
 259 cessed 3D face surface  $\mathbf{S}$ ; column (c) shows the 3D face  $\mathbf{S}$  with extracted  
 260 curves; column (d) shows color-map of the Averageness DSF mapped on  $\mathbf{S}$   
 261 with three poses. The hot colors mean the minimum difference (i.e. maxi-  
 262 mum averageness) and cold colors signify the maximum difference (i.e. min-  
 263 imum averageness). The hotter the color, the higher is the magnitude of the  
 264 averageness.

### 265 3. Gender classification

266 In this work, face averageness and symmetry are different types of infor-  
 267 mation in the 3D facial shapes. Each of them provides a perspective (maybe

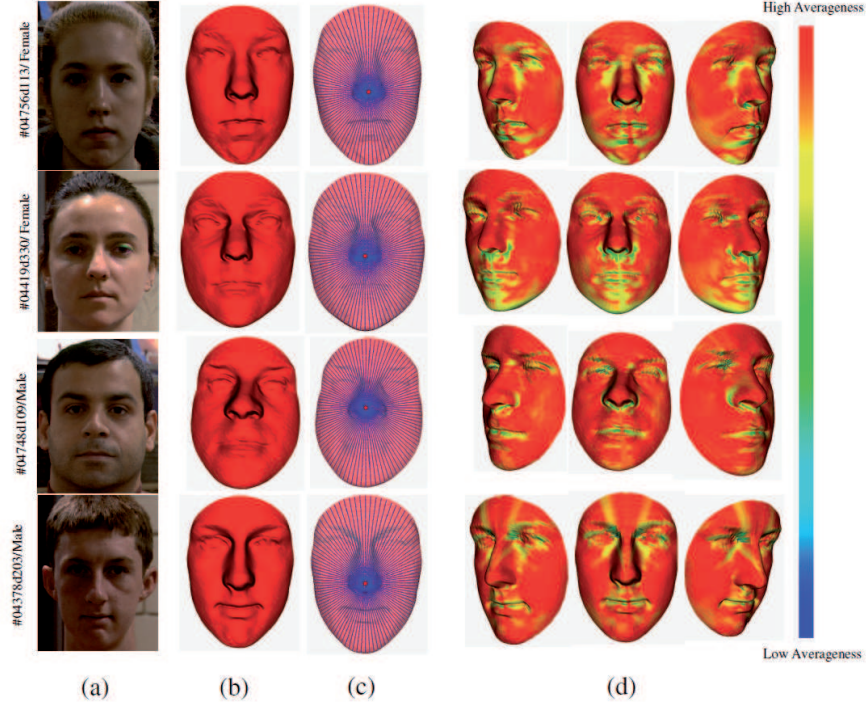


Figure 4: Illustrations of the averageness DSFs on faces. (a) 2D intensity image; (b) preprocessed 3D face surface  $\mathcal{S}$ ; (c) the 3D face  $\mathcal{S}$  with extracted curves; (d) color-map of the Averageness DSF mapped on  $\mathcal{S}$  with three poses. While the cold colors reflect lower averageness, the warm colors represent higher averageness on the face.

correlated perspectives) in face perception. Thus, we first study individually their relationship with gender, then we combine them to find out if it enhances the gender classification results, which means that they contribute to gender classification in different ways. In practice, we use an *early fusion method* which consist in concatenating the *averageness DSF* and *symmetry DSF* features of each scan, to form the *fusion DSF* description. Then, we explore the performance of the Random Forest algorithm with the *avera-*



275 *geness DSF*, the *symmetry DSF* and the *fusion DSF* in different scenarios,  
 276 in combination of Feature Selection methods. It has been demonstrated by  
 277 *Perez et al.* in [29], that different types of information (such as gray scale  
 278 intensity, range image and LBP texture) contributes to face based gender  
 279 classification differently, and the fusion of multi-information yields a better  
 280 classification performance.

### 281 3.1. Feature Selection

282 The size of the features is another important characteristic of the ap-  
 283 proach. As pointed out by *Bekios-Calfa et al.* in [28], in limited computa-  
 284 tional resource contexts, such as the mobiles, the development of resource-  
 285 limited algorithms is important for applications of computer vision and pat-  
 286 tern recognition. In their work, they make use of LDA techniques to reduce  
 287 feature size. In our work, we use feature selection methods to select a much  
 288 smaller set of the features to reduce the computational cost. Compared with  
 289 LDA techniques, feature selection methods do not tranferm the meaning and  
 290 values of feature, thus they allow to track back to the corresponding point  
 291 on the face.

292 Feature subset selection is the process of identifying and removing as  
 293 much irrelevant and redundant information as possible [22]. It is a central  
 294 problem in machine learning. The earliest approaches for feature selection  
 295 were *the filter* methods. These algorithms use heuristics based on general  
 296 characteristics of the data to evaluate the merit of feature subsets. Another  
 297 school of approaches argues that the bias of a particular induction algorithm  
 298 should be taken into account when selecting features. This method, called  
 299 *the wrapper* [23], uses an induction algorithm along with a statistical re-

300 sampling technique such as cross-validation to estimate the final accuracy of  
 301 feature subsets. The filter methods operate independently of any learning  
 302 algorithm. The undesirable features are filtered out of the data before the  
 303 learning begins. They are generally much faster than wrapper methods, es-  
 304 pecially on data of high dimensionality. Since the averageness, symmetry and  
 305 fusion DSFs are really dense and possibly redundant after DSF extraction, we  
 306 use a feature selection procedure on the DSFs to get rid of the irrelevant and  
 307 redundant features. For the merits of filter methods, we chose a filter, named  
 308 Correlation-based-Feature-Selection (CFS) [22]. It is an algorithm that cou-  
 309 ples the evaluation formula based on an appropriate correlation measure and  
 310 a heuristic search strategy. The central hypothesis of CFS is that good fea-  
 311 ture sets should contain features that are highly correlated with the class,  
 312 yet uncorrelated with each other. The feature evaluation formula (Pearsons  
 313 correlation coefficient), based on ideas from test theory, provides an opera-  
 314 tional definition of this hypothesis. Within CFS, we try two heuristic search  
 315 strategies, the Best-First search strategy and the Greedy-Step-Wise search  
 316 strategy. The Best-First search strategy [24] is an AI search strategy that al-  
 317 lows back-tracking along the search path. It moves through the search space  
 318 by greedy hill-climbing augmented with a back-tracking facility. When the  
 319 path being explored becomes non-improving, the Best-First search will back-  
 320 track to a more promising previous subset and continue the search from there.  
 321 The stopping criterion is the number of consecutive non-improving nodes (5  
 322 in our experiments) that result in no improvement. For Greedy-Step-Wise, it  
 323 performs a greedy forward or backward search through the space of attribute  
 324 subsets. It stops when the addition/deletion of any remaining attributes

325 results in a decrease in evaluation.

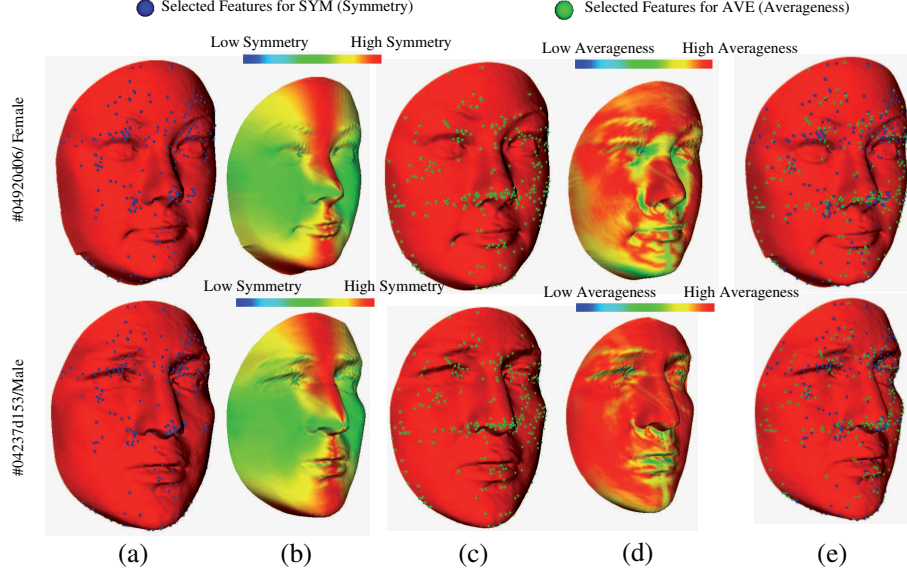


Figure 5: Feature selection. (a) selected points of symmetry DSF in the face; (b) color-map of original symmetry DSF; (c) selected points of averageness DSF in the face; (d) color-map of original averageness DSF; (e) selected points of both averageness DSF and symmetry DSF in face.

326 After Feature selection, we retain 301 salient points for averageness DSF,  
 327 271 salient points for symmetry DSF, and 365 salient points for the fusion.  
 328 The feature selection procedure significantly reduces the size and complexity  
 329 of original DSF description. Figure 5 shows the selected features of aver-  
 330 ageness DSF and symmetry DSF in faces. Column (a) maps the selected  
 331 features of symmetry DSF in the face; Column (b) shows the color-map of  
 332 original symmetry DSF on the face ; Column (c) maps the selected points  
 333 of averageness DSF in the face ; Column (d) shows the original averageness  
 334 DSF on the face; Column (e) maps the selected points of both averageness  
 335 DSF and symmetry DSF in the face. For both averageness DSF and sym-

metry DSF, we observe dense distribution of salient points around the nose and eyes regions. More salient points exist in forehead regions in averageness DSF, and more salient points exist in cheek regions in symmetry DSF. These observations show that averageness DSF and symmetry DSF share both similarities and differences. In other words, they are complementary in face description.

### 3.2. Gender classification based on Random Forest

Face-based gender classification is a binary classification problem which estimates the gender  $c$  of a given test face into Male or Female  $\mathbf{c} \in \{Male, Female\}$ . We carry out gender classification experiments with the well-known machine learning algorithm, Random Forest. Random Forest is an ensemble learning method that grows many classification trees  $t \in \{t_1, \dots, t_T\}$  [25]. To classify a new face from an input vector (DSF-based feature vector  $v = V_\alpha^k$ ), each tree gives a classification result and the forest chooses the classification having the most votes. In the growing of each tree, firstly,  $\mathbf{N}$  instances are sampled randomly with replacement from the original data, to make the training set. Then, if each instance comprises of  $\mathbf{M}$  input variables, a constant number  $\mathbf{m}$  ( $\mathbf{m} \ll \mathbf{M}$ ) is specified. At each node of the tree,  $\mathbf{m}$  variables are randomly selected out of the  $\mathbf{M}$  and the best split on these  $\mathbf{m}$  variables is used to split the node. The process goes on until the tree grows to the largest possible extent, without pruning.

The performance of the forest depends on the correlation between any two trees, and the strength of each individual tree. The forest error rate increases when the correlation decreases, or the strength increases. Reducing  $\mathbf{m}$  reduces both the correlation and the strength. Increasing it increases both.

Thus, an optimal  $\mathbf{m}$  is needed for the trade-off between the correlation and the strength. In Random Forest, the optimal value of  $\mathbf{m}$  is found by using the oob-error rate (out-of-bag-error rate). It is reported that face classification by Random Forest achieves a lower error rate than some popular classifiers, including SVM [20]. As far as we know, there is no reported work in the literature of face-based gender classification using Random Forest.

## 4. Experiments

The FRGCv2 database was collected by researchers from the University of Notre Dame [21] and contains 4007 3D face scans of 466 subjects with differences in gender, ethnicity, age and expression. For gender, there are 1848 scans of 203 female subjects and 2159 scans of 265 male subjects. The ages of subjects range from 18 to 70, with 92.5% in the 18 – 30 age group. When considering ethnicity, there are 2554 scans of 319 White subjects, 1121 scans of 99 Asian subjects, 78 scans of 12 Asian-southern subjects, 16 scans of 1 Asian and Middle-east subject, 28 scans of 6 Black-or-African American subjects, 113 scans of 13 Hispanic subjects, and 97 scans of 16 subjects whose ethnicity are unknown. About 60% of the faces have a neutral expression, and the others show expressions of disgust, happiness, sadness and surprise. All the scans in FRGCv2 are near-frontal. With this dataset, we conducted two experiments. The first one is to examine the robustness of our approach to age and ethnicity variations. It uses the 466 earliest scan of each subject in FRGCv2, of which more than 93% are neutral-frontal. The second one extends to examine the robustness of our approach to variations of expression. It considers all the 4007 scans in FRGCv2, about

385 40% of which are expressive faces. For these experiments, the results are  
386 generated in a subject-independent fashion, using a 10-fold cross-validation  
387 setup.

#### 388 4.1. Data preprocessing

389 The 3D face models present some imperfections, such as the holes (caused  
390 by the absorption of the laser in the dark areas like eyebrows and eyes and  
391 by the self-occlusions), the hair, and the spikes (caused by acquisition noise).  
392 Thus, a preprocessing step is needed to limit their influence. Firstly, through  
393 boundary detection, link-up and triangulation, holes are filled in each scan.  
394 Secondly, since the scans in FRGCv2 are all near-frontal, the nose tip is de-  
395 tected with a simple algorithm. The nose tip is detected by analyzing the  
396 peak point of the face scan in the depth direction. Then, the mesh is cropped  
397 with a sphere centered at the nose tip to discard the hair and the neck re-  
398 gions. Finally, a smoothing filter is used to distribute evenly the 3D vertices  
399 which capture the original 3D shape. We next perform the well-known Iter-  
400 ative Closest Point (ICP) algorithm to normalize the poses of the obtained  
401 meshes according to a reference mesh (frontal). The symmetry plane is then  
402 picked up as the plane that has as origin the nose tip and has an horizontal  
403 normal. In practice, the preprocessing step is performed automatically on  
404 the whole FRGCv2 dataset without any manual intervention. We obtained  
405 4005 well preprocessed scans after preprocessing. The failed two scans (with  
406 scan id 04629d148 and 04815d208) were resulted from wrong nose tip detec-  
407 tion. Considering the ratio of failure is rather tiny ( $2/4007 < 0.0005$ ), we omit  
408 the influence of the two failed scans for the results generation.

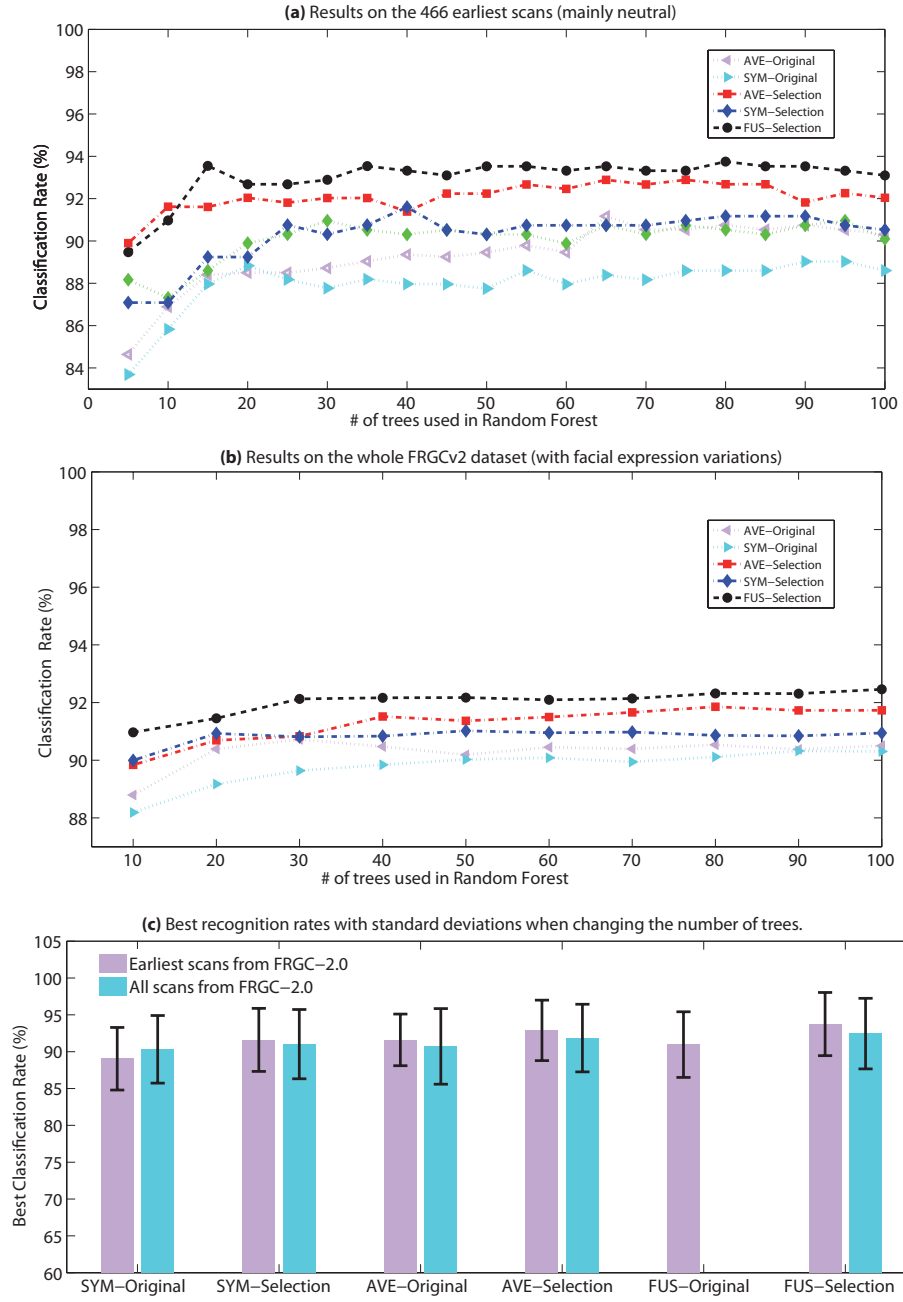


Figure 6: The reported results of the proposed methods<sup>1</sup>using Random Forest with different number of trees.

#### 4.2. Robustness to variations of age and ethnicity

Among the 466 earliest scans, 431 scans are neutral-frontal and 35 are expressive-frontal. In our 10-fold cross validation setup, the 466 scans are randomly partitioned into 10 folds with each fold containing 46 – 47 scans. In each round, 9 of the 10 folds are used for training while the remaining fold is used for testing. The average recognition rate and standard deviation for 10 rounds then give a statistically significant performance measure. The relationship between the gender classification result and the number of trees used in the Random Forest is depicted in Figure 6(a). It demonstrates that a significant relationship exists between gender and facial averageness and facial symmetry considered separately. We note also that both the fusion and the feature selection improve the gender classification results. In fact, the fusion descriptor outperforms individual averageness and symmetry descriptor. This implies that facial averageness and symmetry relate to gender in different ways. At the same time, results after the feature selection always override the results without feature selection. This means that the original averageness DSF and symmetry DSF contain redundant information. Gender-related features are distributed unequally in the facial regions. The best gender classification rate is 93.78%, achieved by 80-Tree Random Forest with the fusion descriptor after feature selection. This result is detailed in the confusion matrix in Table 1. The recognition rate for females (92.02%) is

---

<sup>1</sup>Methods as described in Figure 1 : (1) the symmetry DSF features (*SYM-Original*), (2) the selected features of symmetry DSF features (*SYM-Selection*), (3) the averageness DSF features (*AVE-Original*), (4) the selected features of averageness DSF features (*AVE-Selection*), (5) the fusion of symmetry and averageness DSF features by concatenation (*FUS-Original*), and (6) the selected features of the fusion of symmetry and averageness DSF features (*FUS-Selection*).



430 slightly lower than for male ones (95.44%). It is probably due to the fact that  
431 more male faces were used for training. We also performed a 10-fold 100-  
432 repetition experiment with Random Forest under the same setting, which  
433 resulted at an average classification rate of 92.84% with a standard deviation  
434 of 3.58%.

Table 1: Confusion matrix of RF-based classification.

%	Female	Male
Female	91.63	8.37
Male	4.56	95.44
<i>Recognition Rate = 93.78 ± 4.29%</i>		

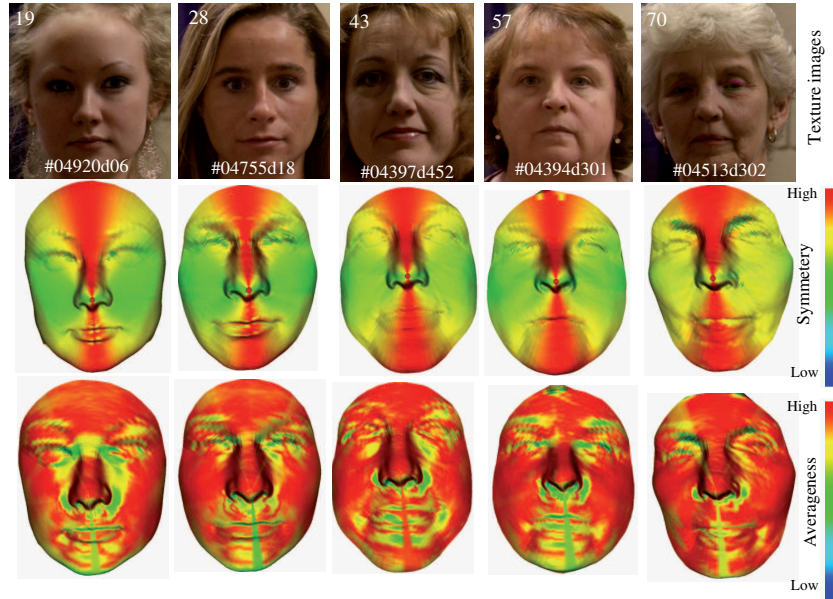


Figure 7: DSFs on faces with different Age.

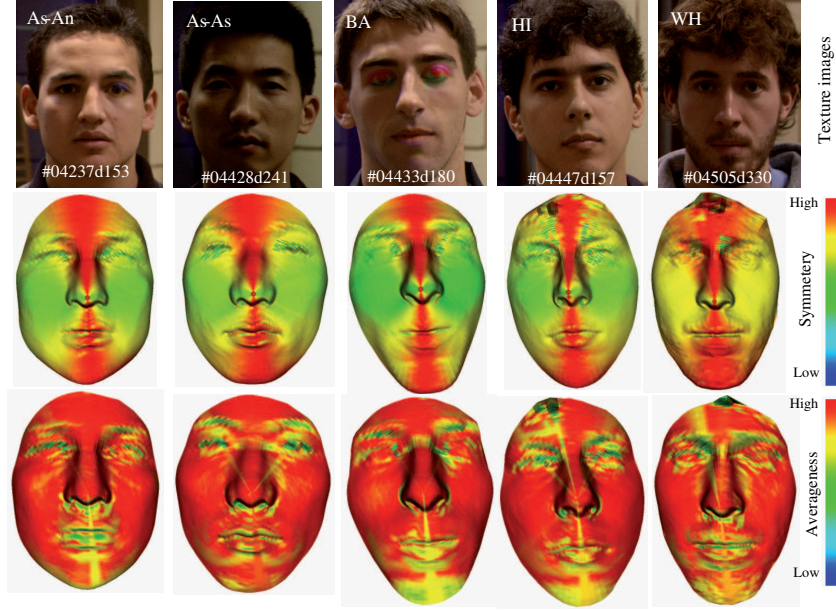


Figure 8: DSFs on faces with different Ethnicity.

Figure 7 illustrates the color-maps of symmetry DSF and averageness DSF on female faces with age differences and Figure 8 illustrates the color-maps of symmetry DSF and averageness DSF on male faces with differences in ethnicity. The information related to age, ethnicity and identity of scans are presented in the 2D images in the upper row of each figure. Based on the middle rows of Figure 7 and Figure 8, we can observe that the bilateral symmetry of both genders convey a visually symmetrical pattern, where the color-map of left-face is globally in symmetry with the right-face, although subtle local asymmetry exists. Low-level deformations (red color) are usually located near the middle plane and high-level deformations (yellow and green colors) happen more frequently in further areas. The asymmetry, in female faces, change obviously more smoothly than in male faces. On the other

hand, with the lower rows of Figure 7 and Figure 8, we observe that female faces exhibit more deformations in mouth, nose and eye regions to deform from the averageness face template. More subtly, in cheek and forehead regions, the color is more consistent in male faces. All of these observations above stay relatively consistent with changes of age and ethnicity. We believe that these common patterns contribute to the robustness of our approach to variations of age and ethnicity to some extent.

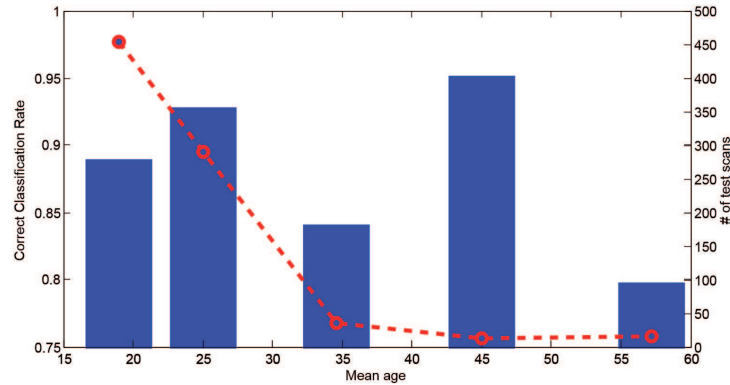


Figure 9: Gender classification results of different age group (the blue bars show the average recognition rate of each age group, and the red line shows the number of scans in this age group).

As it is well known that face perception is strongly affected by age [30], we provide Figure 9 to analyze gender classification performance for different age groups. In this figure, the blue bars show the average recognition rate for each age group, and the red line shows the number of scans in the same age group. We could confirm that gender classification is strongly influenced by the age. Generally, although the gender classification results decrease from above 90% to about 80% when increasing the age, all these results are near or

461 above 80%. That is to say the performance of our approach stays relatively  
 462 high with age variation. Moreover, due to unbalanced age distribution of  
 463 scans in FRGCv2 dataset, we see the number of scans decreased significantly  
 464 when the age is increased. We assume that this is also a reason for the  
 465 decrease of the gender classification results.

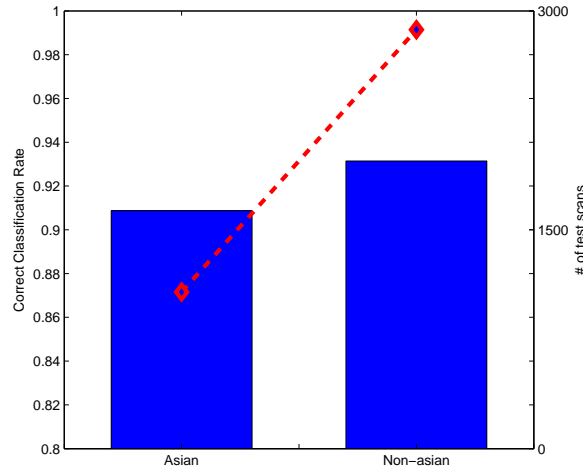


Figure 10: Gender classification results of different ethnicity group (the blue bars show the average recognition rate of each age group, and the red line shows the number of scans in this ethnic group).

466 Figure 10 analyzes the relationship between the obtained classification  
 467 rate when varying the ethnicity. Here, the whole FRGCv2 dataset is sepa-  
 468 rated into Asian and Non-Asian groups. We can see that the gender clas-  
 469 sification rates, shown by the blue bars, stay above 90% when varying the  
 470 ethnicity. The classification rate of Non-Asian group is 3 – 4 percent higher  
 471 than that of the Asian group. This is probably due to a more sufficient train-  
 472 ing step has been involved with Non-Asian group, since it contains more than

two times of the number of the scans of the Asian group, as shown in the figure by the red line.

#### 4.3. Robustness to expression variations

In this experiment, with all the preprocessed scans of FRGCv2, we first performed the DSF extraction for averageness, symmetry and fusion descriptors, and then did the 10-fold subject-independent cross-validation with Random Forest. For each round, the scans of 46 subjects are randomly selected for testing, and the scans of the remaining subjects are dedicated to the training. For all the 10 rounds of experiments, no common subjects are used in training/testing. The relationship between the classification result and the number of trees used in Random Forest is shown in Figure 6(b). We note again that both fusion and feature selection improve the results. The best result achieved with the fusion and feature selection is  $92.46\% \pm 4.79$  with 100-Tree Random Forest. We argue this result by the fact that the majority of the selected features are located on the facial areas which are less affected by the expressions in particular the nose, the eyebrows, and the forehead as illustrated in Figure 5. Considering the FRGCv2 dataset is a challenging dataset which contains as many as 4007 scans with various changes in age, ethnicity and expression, we claim even more confident that a significant relationship exists between gender and 3D facial averageness/symmetry, and our method is effective and robust to ethnicity and expression variations.

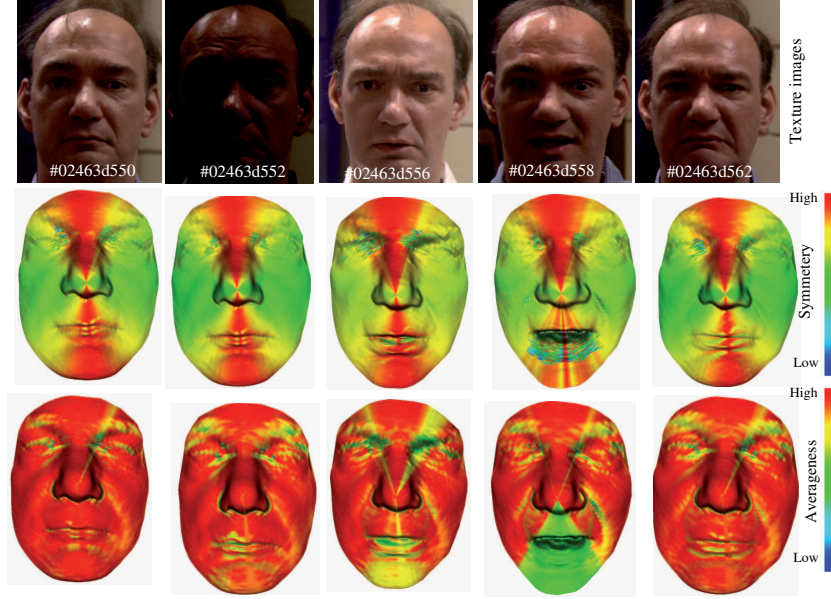


Figure 11: DSFs on faces with different expressions.

Figure 11 shows color-maps of DSFs generated for a subject with different expressions. Similar to the observations in Figure 7 and Figure 8, we perceive again in the middle row of Figure 11 that the symmetry deformations on both sides of the face are globally in symmetry, although tiny local asymmetry exists in areas like eye corners and lips. Low-level deformations (red) always locate near the middle plane and high-level deformations (yellow and green) occur more frequently in farther areas. With the lower rows of Figure 7 and Figure 11, we observe again that female faces require more deformation in mouth, nose and eye regions to deform from the averageness face template. In cheek and forehead regions, the color is more consistent in male faces. All these visible patterns do not change significantly with expression variations. We assume that these patterns contribute to the robustness

506 of our approach to expression changes. Figure 6(c) shows the best gender  
 507 recognition results (shown as bars) and their standard deviation (shown as  
 508 black lines) in our experiment. It shows that the gender recognition rate  
 509 increases with both fusion and feature selection, and the performances of all  
 510 the approaches change little between the 466 earliest scans protocol and the  
 511 whole FRGCv2 dataset protocol. It means our approach is even relatively  
 512 robust to the size of the training set.

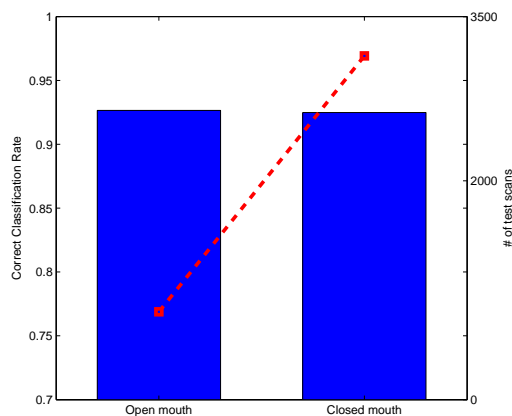


Figure 12: Gender classification results of different expression group (the blue bars show the average recognition rate of each age group, and the red line shows the number of scans in this expression group).

513 Again, in Figure 12, we illustrate the effects of expression variations on  
 514 the proposed approach. We separated the FRGCv2 dataset into Open-mouth  
 515 and Closed-mouth groups. Despite the fact of the unbalanced number of  
 516 training scans in Open-mouth and Closed-mouth groups, as shown by the  
 517 red line, the results shown by the blue bars in the figure are all above 90%,  
 518 and the results between these two groups are comparable with each other.

#### 519 4.4. Comparison with state of the art

520 Table 2 gives a comparison of this work with previous studies in 3D-based  
521 gender classification. With differences in the dataset, landmarking, exper-  
522 iment settings and so on, it is difficult to compare and rank these works  
523 simply according to the result values. Compared with our work, works in [9],  
524 [14], [15] are based on relatively smaller dataset which leave doubts about the  
525 statistical significance of their performances on larger and more challenging  
526 datasets. Works in [9], [12], [14], [15] require manual landmarking, thus they  
527 are not fully-automatic. Works in [9], [14], [15], [16] use different experi-  
528 mental settings other than the most prevailing 10-fold cross-validation. Our  
529 work addressed gender classification in a fully automatic way without man-  
530 ual landmarking. Experimented on a large dataset, FRGCv2, which contains  
531 challenging variations in expression, age and ethnicity, and reached competi-  
532 tive results with literature. The nearest works to ours are done by *Ballihi et*  
533 *al.* in [17] and *Toderici et al.* in [3]. With the 466 Earliest scans of FRGCv2  
534 and standard 10-fold cross-validation, *Ballihi et al.* achieved 86.05% classifi-  
535 cation rate, while we achieved a much higher result of 93.78% by combining  
536 facial shape averageness and bilateral asymmetry. In [3], *Toderici et al.* also  
537 performed automatic 10-fold cross-validation on the FRGCv2 dataset in a  
538 subject-independent fashion. In general, we have achieved comparable re-  
539 sults than them. They achieve about 1% higher gender classification rate  
540 than us. While we achieve a lower standard deviation which signifies better  
541 stability of the algorithm than theirs<sup>2</sup>.

---

<sup>2</sup>During the work, we found 8 scans of a subject (id 04662, female indeed) had been mislabeled as male in the FRGCv2 metadata. We corrected them before the experiments.



Table 2: Comparison of our approach to earlier studies.

<i>Reference</i>	<i>Dataset</i>	<i>Auto</i>	<i>Features</i>	<i>Classifiers</i>	<i>Experiment settings</i>	<i>Results</i>	<i>Shape/Texture</i>
<i>Ballihi et al. [17]</i>	466 earliest scans of FRGCv2	Yes	facial curves	Adaboost	10-fold cross-validation	86.05%	Shape
<i>Toderici et al. [3]</i>	All scans of FRGCv2	Yes	Wavelets	Polynomial-SVM	10-fold cross-validation	Male : $94 \pm 5\%$ Female : $93 \pm 4\%$	Shape
<i>Hu et al. [16]</i>	729 UND scans and 216 private scans	Yes	Curvature based shape index	RBF-SVM	5-fold cross-validation	94.03%	Shape
<i>Han et al. [14]</i>	61 3D scans in GavabDB	No	Geometry Features	RBF-SVM	5-fold cross-validation	$82.56 \pm 0.92\%$	Shape
<i>Wu et al. [15]</i>	Needle maps of 260 subjects from UND	No	PGA features	Posterior Probability	200 train/60 test, 6 repetitions	$93.6 \pm 4\%$	Shape+Texture
<i>Lu et al. [12]</i>	1240 scans from UND and MSU	No	Grid element values	Posterior Probability	10-fold cross-validation	$91 \pm 3\%$	Shape+Texture
<i>Liu et al. [9]</i>	111 full 3D scans of 111 subjects	No	Variance Ratio in HD and OD faces	linear classifier	half train/half test, 100 repetitions	HD: $91.16 \pm 3.15\%$ OD: $96.22 \pm 2.30\%$	Shape
<i>Our work<sup>1</sup></i>	466 earliest scans of FRGCv2	Yes	AVE+SYM DSFs	Random Forest	10-fold cross-validation	$93.78 \pm 4.29\%$	Shape
<i>Our work<sup>2</sup></i>	All scans of FRGCv2	Yes	AVE+SYM DSFs	Random Forest	10-fold cross-validation	$92.46 \pm 3.58\%$	Shape

## 5. Conclusion

In this paper, we have proposed a fully automatic approach based on 3D facial averageness/symmetry differences for gender classification. We have proposed to use our *Dense Scalar Fields* grounding on Riemannian Geometry to capture densely facial averageness and its bilateral symmetry. The remaining challenge is the large dimensionality of the DSFs, which is handled using a feature-selection-based dimension reduction, followed by a Random Forest classifier. Despite the wide range of age, ethnicity and facial expressions, our method achieves a gender classification result of  $93.78\% \pm 4.29\%$  with 466 earliest scans of subjects, and  $92.46\% \pm 3.58$  on the whole

552 FRGCv2 dataset. We have also demonstrated that a significant relationship  
553 exists between the gender and these two high-level cues in face perception,  
554 the face averageness and symmetry. Our approach is competitive with state-  
555 of-the-art approaches. One of the limitations of the proposed approach is the  
556 dependence on near-frontal pose of faces to compute the symmetry and the  
557 averageness DSFs.

## 558 References

- 559 [1] A. Cellerino and D. Borghetti and F. Sartucci, "Sex differences in face  
560 gender recognition in humans", *Brain Research Bulletin*, vol. 63, 2004,  
561 pp. 443-449.
- 562 [2] V. Bruce and AM. Burton and E. Hanna and P. Healey and O. Mason  
563 and A. Coombes and R. Fright and A. Linney, "Sex discrimination: how  
564 do we tell the difference between male and female faces?", *Perception*,  
565 vol. 22, 1993, pp. 131152..
- 566 [3] G. Toderici and S. O'Malley and G. Passalis and T. Theoharis and  
567 I. Kakadiaris, "Ethnicity- and Gender-based Subject Retrieval Using  
568 3-D Face-Recognition Techniques", *International Journal of Computer*  
569 *Vision*, vol. 89, 2010, pp. 382-391.
- 570 [4] J. Ylioinas and A. Hadid and M. Pietikinen, "Combining Contrast In-  
571 formation and Local Binary Patterns for Gender Classification", *Image*  
572 *Analysis*, vol. 6688, 2011, pp. 676-686.
- 573 [5] E. Makinen and R. Raisamo, "An experimental comparison of gender

- 574 classification methods", *Pattern Recognition Letters*, vol. 29, 2008, pp.  
575 1544-1556.
- 576 [6] W. Yang and C. Chen and K. Ricanek and C. Sun, Changyin, "Gender  
577 Classification via Global-Local Features fusion", *Biometric Recognition*,  
578 vol. 7098, 2011, pp. 214-220.
- 579 [7] C. Shan, "Learning local binary patterns for gender classification on  
580 real-world face images", *Pattern Recognition Letters*, vol. 33, 2012, pp.  
581 431-437.
- 582 [8] N. Kumar and A. Berg and P.N. Belhumeur and S. Nayar, "Describ-  
583 able Visual Attributes for Face Verification and Image Search", *Pattern*  
584 *Analysis and Machine Intelligence*, vol. 33, 2008, pp. 1962 -1977.
- 585 [9] Y. Liu and J. Palmer, "A quantified study of facial asymmetry in 3D  
586 faces", *Analysis and Modeling of Faces and Gestures*, 2003, pp. 222-229.
- 587 [10] LG. Farkas and G. Cheung, "Facial asymmetry in healthy North Amer-  
588 ican Caucasians. An anthropometrical study", *Angle Orthod*, vol. 51,  
589 1981, pp. 70-77.
- 590 [11] A. Little and B. Jones and C. Waitt and B. Tiddeman and D. Feinberg  
591 and D. Perrett and C. Apicella and F. Marlowe, "symmetry Is Related to  
592 Sexual Dimorphism in Faces: Data Across Culture and Species", *PLoS*  
593 *ONE*, vol. 3, 2008, pp. e2106 .
- 594 [12] X. Lu and H. Chen and A. Jain, "Multimodal facial gender and ethnic-  
595 ity identification", *Proceedings of the 2006 international conference on*  
596 *Advances in Biometrics*, 2006, pp. 554-561.

- 597 [13] "The main differences between male and female faces",  
598 *www.virtualffs.co.uk*.
- 599 [14] X. Han and H. Ugail and I. Palmer, "Gender Classification Based on 3D  
600 Face Geometry Features Using SVM", *CyberWorlds*, 2009, pp. 114-118.
- 601 [15] J. Wu and W. A. P. Smith and E. R. Hancock, "Gender Classification  
602 using Shape from Shading", *International Conference on Image Analysis  
603 and Recognition*, 2007, pp. 499-508.
- 604 [16] Y. Hu and J. Yan and P. Shi, "A fusion-based method for 3D facial gen-  
605 der classification", *Computer and Automation Engineering (ICCAE)*,  
606 vol. 5, 2010, pp. 369-372.
- 607 [17] L. Ballihi and B. Ben Amor and M. Daoudi and A. Srivastava and  
608 D. Aboutajdine, "Boosting 3D-Geometric Features for Efficient Face  
609 Recognition and Gender Classification", *IEEE Transactions on Infor-  
610 mation Forensics & Security*, vol. 7, 2012, pp. 1766-1779.
- 611 [18] H. Drira and B. Ben Amor and M. Daoudi and A. Srivastava and S.  
612 Berretti, "3D Dynamic Expression Recognition based on a Novel Deform-  
613 ation Vector Field and Random Forest", *21st International Conference  
614 on Pattern Recognition*, 2012.
- 615 [19] A. Srivastava and E. Klassen and S. H. Joshi and I. H. Jermyn, "Shape  
616 Analysis of Elastic Curves in Euclidean Spaces", *Pattern Analysis and  
617 Machine Intelligence*, vol. 33, 2011, pp. 1415 -1428.

- 618 [20] A. Z. Kouzani and S. Nahavandi and K. Khoshmanesh, "Face classification by a random forest", *TENCON 2007-2007 IEEE Region 10 Conference*, 2007, pp. 1-4.
- 619
- 620
- 621 [21] P. J. Phillips and P. J. Flynn and T. Scruggs and K. W. Bowyer and J. Chang and K. Hoffman and J. Marques and J. Min and W. Worek, "Overview of the face recognition grand challenge", *Computer Vision and Pattern Recognition*, vol. 1, 2005, pp. 947 - 954.
- 622
- 623
- 624
- 625 [22] Mark A. Hall, "Correlation-based Feature Subset Selection for Machine Learning", *PhD thesis, Department of Computer Science, University of Waikato*, 1999, chapter 3-4.
- 626
- 627
- 628 [23] R. Kohavi, "Wrappers for Performance Enhancement and Oblivious Decision Graphs". *PhD thesis, Stanford University*, 1995, chapter 4.
- 629
- 630 [24] E. Rich and K. Knight, "Artificial Intelligence", *McGraw-Hill College*, 1991.
- 631
- 632 [25] L. Breiman, "Random Forests", *Machine Learning*, vol. 45, 2001, pp 5-32.
- 633
- 634 [26] Lines PA, Lines RR, Lines CA., "Profilmetrics and facial esthetics". *Am J Orthod*, 1978, 73:640-57.
- 635
- 636 [27] Bradley N. Lemke, "Surgical Anatomy of the Face". *Arch Ophthalmol*, 1995, 113(8):982.
- 637
- 638 [28] Bekios-Calfa J, Buenaposada JM, Baumela L., "Revisiting linear dis-

- 639       criminant techniques in gender recognition". *IEEE Trans Pattern Anal*  
640       *Mach Intell*, 2011 Apr, 33(4):858-64.
- 641   [29] C. Perez, J. Tapia, P. Estvez, C. Held., "Gender Classification From Face  
642       Images Using Mutual Information and Feature Fusion". *International*  
643       *Journal of Optomechatronics - INT J OPTOMECHATRONICS*, 2012,  
644       vol. 6, no. 1, pp. 92-119.
- 645   [30] Ferrario VF, Sforza C, Ciusa V, Dellavia C, Tartaglia GM, "The effect  
646       of sex and age on facial asymmetry in healthy subjects: a cross-sectional  
647       study from adolescence to mid-adulthood", *J Oral Maxillofac Surg*, 2001  
648       Apr, 59(4):382-8.